


## Article

# Discovery Potent of Thiazolidinedione Derivatives as Antioxidant, $\alpha$ -Amylase Inhibitor, and Antidiabetic Agent

Manal Y. Sameeh<sup>1,\*</sup>, Manal M. Khowdiary<sup>1,2</sup>, Hisham S. Nassar<sup>3,4</sup>, Mahmoud M. Abdelall<sup>4</sup>, Suliman A. Alderhami<sup>3</sup> and Ahmed A. Elhenawy<sup>3,4,\*</sup> 

<sup>1</sup> Chemistry Department, Faculty of Applied Science, Alleeth University Collage, Umm Al-Qura University, Makkah 24211, Saudi Arabia; mmkhowdiary@uqu.edu.sa

<sup>2</sup> Applied Surfactant Laboratory, Egyptian Petroleum Research Institute, Nasr City 11727, Cairo, Egypt

<sup>3</sup> Department of Chemistry, Faculty of Science and Arts in Al-Mukhwah, Al-Baha University, Al-Mukhwah 65311, Saudi Arabia; hishamsan@bu.edu.sa (H.S.N.); Alderhami@bu.edu.sa (S.A.A.)

<sup>4</sup> Chemistry Department, Faculty of Science, Al-Azhar University, Nasr City 11884, Cairo, Egypt; mohmoed@azhar.edu.eg

\* Correspondence: ahmed.elheawy@azhar.edu.eg or elhenawy\_sci@hotmail.com (A.A.E.); Myassemih@uqu.edu.sa (M.Y.S.); Tel.: +966-50-8678-586 (A.A.E.)

**Abstract:** This work aimed to synthesize safe antihyperglycemic derivatives bearing thiazolidinedione fragment based on spectral data. The DFT theory discussed the frontier molecular orbitals (FMOs), chemical reactivity of compounds, and molecular electrostatic potential (MEP) to explain interaction between thiazolidinediones and the biological receptor.  $\alpha$ -amylase is known as the initiator-hydrolysis of the of polysaccharides; therefore, developing  $\alpha$ -amylase inhibitors can open the way for a potential diabetes mellitus drug. The molecular docking simulation was performed into the active site of PPAR- $\gamma$  and  $\alpha$ -amylase. We evaluated in vitro  $\alpha$ -amylase's potency and radical scavenging ability. The compound **6** has the highest potency against  $\alpha$ -amylase and radical scavenging compared to the reference drug and other members. They have been applied against anti-diabetic and anti-hyperlipidemic activity (in vivo) based on an alloxan-induced diabetic rat model during a 30-day treatment protocol. The most potent anti hyperglycemic members are **6** and **11** with reduction percentage of blood glucose level by 69.55% and 66.95%, respectively; compared with the normal control. Other members exhibited moderate to low anti-diabetic potency. All compounds showed a normal value against the tested biochemical parameters (CH, LDL, and HDL). The ADMET profile showed good oral bioavailability without any observed carcinogenesis effect.

**Keywords:** thiazolidinedione; anti-diabetic; antioxidant; molecular docking



**Citation:** Sameeh, M.Y.; Khowdiary, M.M.; Nassar, H.S.; Abdelall, M.M.; Alderhami, S.A.; Elhenawy, A.A. Discovery Potent of Thiazolidinedione Derivatives as Antioxidant,  $\alpha$ -Amylase Inhibitor, and Antidiabetic Agent. *Biomedicines* **2022**, *10*, 24. <https://doi.org/10.3390/biomedicines10010024>

Academic Editor: Paola Pontrelli

Received: 30 November 2021

Accepted: 21 December 2021

Published: 23 December 2021

**Publisher's Note:** MDPI stays neutral with regard to jurisdictional claims in published maps and institutional affiliations.



**Copyright:** © 2021 by the authors. Licensee MDPI, Basel, Switzerland. This article is an open access article distributed under the terms and conditions of the Creative Commons Attribution (CC BY) license (<https://creativecommons.org/licenses/by/4.0/>).

## 1. Introduction

Diabetes mellitus (DM) is a common chronic health problem, with about 416 million people worldwide suffering from DM. This figure is expected to increase by 2040 to 618 million cases [1–4]. The DM is classified into two major classes: as “DMI” and “DMII” [5,6]. About >90% of individuals suffer from DMII (non-insulin-dependent diabetes mellitus; “NIDDM”). The researchers recognized DMII by tissue resistance to the action of insulin combined with a reduction in insulin secretion due to resistance or deficiency regarding beta cells [6].

An increased blood glucose level is linked to raising several health problems, including cardiovascular disease, further insulin damage, and so on. DMII patients have a higher risk of developing cardiovascular disease than non-DM patients [7].  $\alpha$ -glucosidase and  $\alpha$ -amylase are vital enzymes in the therapy process [8], and responsible for breakdown of  $\alpha$ -D-(1,4)-glycosidic bond in starch to get monosaccharides [9]. The inhibition of these enzymes offers an effective protocol for reducing blood glucose level [7,10]. PPAR- $\gamma$  (peroxisome proliferator-activated receptor) is an essential component in adipogenesis. It also serves a vital function via sensitivity to insulin, organization of the cell cycle, and

cell-differentiation. The nuclear receptor family (NR1C3) includes PPAR- $\gamma$  known as the glitazone receptor, which organizes the gene expression involved in glucose metabolism [11]. The clinical study showed that a mixed therapy involving  $\alpha$ -glucosidase inhibitors and PPAR- $\gamma$ -agonists [12–14] was a helpful strategy for the treatment of DMII, as acarbose mixed with pioglitazone. Acarbose prevents NIDDM, and reduces cardiovascular problem [15]. While pioglitazone decreases cardiovascular action and anti-atherosclerosis [16]. The pre-clinical results of rosiglitazone and pioglitazone revealed no negative effects throughout the short periods of therapy (30 or 48 days), but did exhibit side effects after prolonged periods of use (years). Thus, in this work, we hope to synthesize new compounds without or with low toxicity when applied as antidiabetic medication. However, future trials with prolonged compounds consumption will be conducted, and the results will be published.

Thiazolidinediones (TZDs) are an efficient DMII drug [17], (Figure 1). The combination therapy is also efficient for older patients that have hypertension, DMII [18], and induced-electrolyte-disturbance in rats with DMII [19]. Despite the efficiency of the drugs currently in use, such as acarbose and TZDs, they are associated with adverse side effects, such as diarrhea and obesity. The investigation of a more effective novel drug with low side effects is a valuable target [20]. Recently, uni-molecular and multi-target drugs have been developed to treat metabolic-syndrome, such as the inhibitor of Na-dependent-glucose-transporters “SGLTI” [21,22].

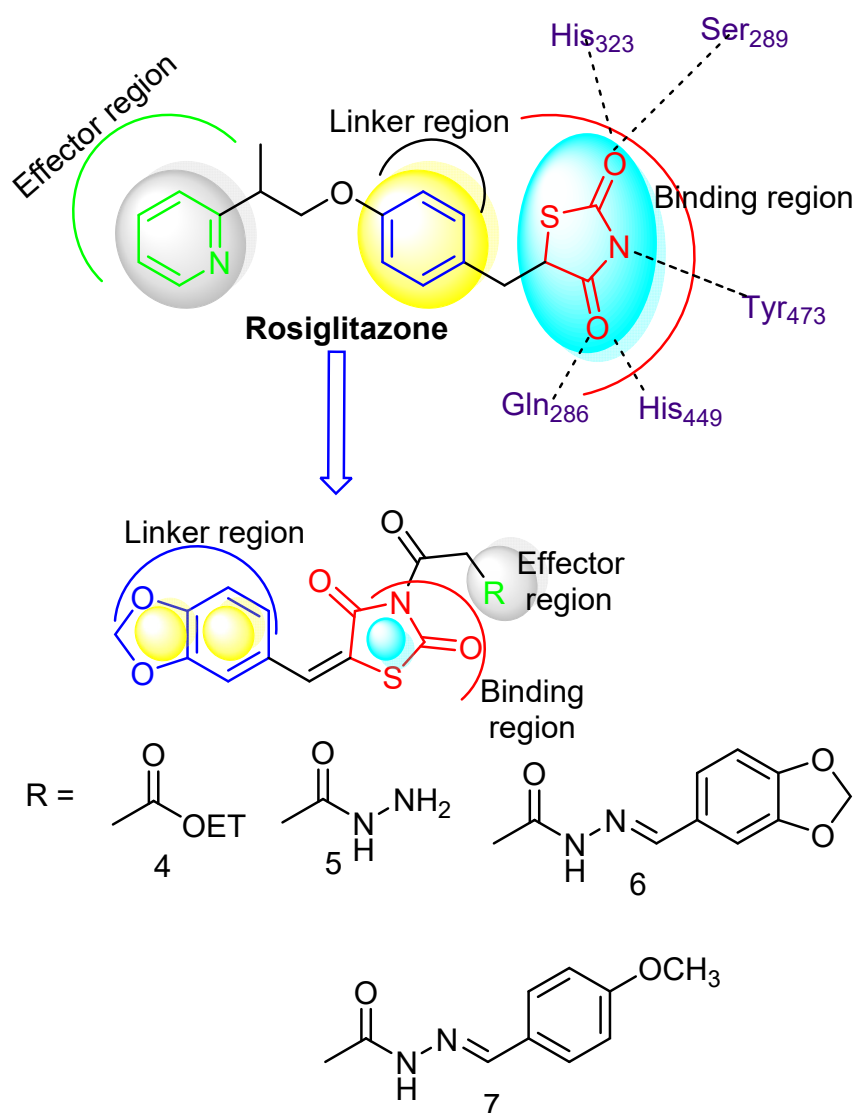


**Figure 1.** Designed molecule compliance of rosiglitazone pharmacophore.

TZDs are hepatotoxic and carcinogenic, as well as being associated with dangerous side effects, such as oedema, obesity, and cardiac problems [23,24]. The 2,4-thiazolidinediones have several potential profiles against anticancer [25], anti-oxidant [26], anti-malarial [27], anti-obesity, and anti-microbial activities [27,28].

In view of the above mentioned facts, we reported the discovery of potent new synthetic thiazolidinedione derivatives as  $\alpha$ -amylase inhibitors and antioxidants in vitro, and evaluation of in vivo anti-diabetic and antihyperlipidemic activity. We performed docking study also to gain further insights concerning the possible binding modes of our compounds.

## 2. Materials and Methods

Melting points, thin layer chromatography ( $R_f$ ), IR, NMR, elemental analyses (C, H, N), and mass spectra were recorded (Supplementary Figure S1). This study obeyed to standards of the ethics committee for the National Research center which complies with the National Regulations on Animal Welfare and Institutional Animal Ethical Committee (IAEC).

### 2.1. Chemistry

#### 2.1.1. Interaction of the Potassium Salt 3 with Halogenated Compounds

The proper halogenated compounds as chloroacetone and chloroacetic acid (0.1 mol) were refluxed with **3** (0.1 mol) in DMF (50 mL) to give **5**, **6**, respectively. The crude products were separated and crystallized from the appropriate solvent.

*5-(benzo[d][1,3]dioxol-5-ylmethylene)-3-(2-oxopropyl) thiazolidine-2,4-dione (5)*. Pale yellow crystals, yield 67%, m.p. 171–173 °C. IR (KBr): ( $\nu/\text{cm}^{-1}$ ) = 1691, 1737 (CO).  $^1\text{H-NMR}$  (DMSO- $d_6$ )  $\delta$  = 7.79 (s, 1H, CH = benzyldine), 7.20–7.14 (m, 1H-ArH), 7.10 (dd,  $J$  = 1.9, 0.5 Hz, 1H, ArH), 7.02 (d,  $J$  = 8.9 Hz, 1H, ArH), 6.01 (s, 2H, CH<sub>2</sub> dioxole), 4.59 (s, 2H), 2.18 (s, 3H).  $^{13}\text{C NMR}$  (DMSO- $d_6$ )  $\delta$  201.41, 170.00, 168.67, 149.34, 148.33, 130.68, 128.12, 125.32, 119.76, 110.52, 109.65, 101.85, 48.74, 27.10. Anal. Calcd for C<sub>14</sub>H<sub>11</sub>NO<sub>5</sub>S (305): C, 55.08; H, 3.60; N, 4.59. Found: C, 55.03; H, 3.56; N, 4.53.

*2-(5-(benzo[d][1,3]dioxol-5-ylmethylene)-2,4-dioxothiazolidin-3-yl)acetic acid (6)*. Yellow crystals, yield 71%, m.p. 188–190 °C. IR (KBr): ( $\nu/\text{cm}^{-1}$ ) = 3421 (OH), 1711, 1744 (C = O).  $^1\text{H-NMR}$  (DMSO- $d_6$ )  $\delta$  9.93 (s, 1H, OH), 7.81–7.77 (m, 1H, CH = benzyldine), 7.20–7.14 (m, 1H, Ar-H), 7.10 (dd,  $J$  = 1.9, 0.5 Hz, 1H, Ar-H), 7.02 (d,  $J$  = 8.9 Hz, 1H, Ar-H), 6.01 (s, 2H, CH<sub>2</sub> dioxole), 4.65 (s, 2H).  $^{13}\text{C NMR}$  (DMSO- $d_6$ ) 170.51, 170.14, 168.51, 149.34, 148.33, 130.72, 128.12, 125.32, 119.76, 110.52, 109.65, 101.85, 41.71. Anal. Calcd for C<sub>13</sub>H<sub>9</sub>NO<sub>6</sub>S (307): C, 50.81; H, 2.93; N, 4.56. Found: C, 50.77; H, 2.91; N, 4.51.

#### 2.1.2. 2-(5-(Benzo[d][1,3]dioxol-5-ylmethylene)-2,4-dioxothiazolidin-3-yl)-2-oxoethyl (5-Methyl-1,3,4-thiadiazol-2-yl) Carbamodithioate (9)

The carbon disulfide was added to 5-methyl-1,3,4-thiadiazol-2-amine (**7**; 0.01 mol.) in the potassium hydroxide solution to give the corresponding potassium salt (**8**). The compound (**4**; 0.01 mol) was added, then the reaction mixture was stirred for 3 h, then diluted with water. The precipitate was collected, and finally recrystallized from acetic acid to afford the compound **9** as yellow crystals, yield 69%, m.p. 261–262 °C. IR (KBr): ( $\nu/\text{cm}^{-1}$ ) = 1698, 1742 (CO).  $^1\text{H-NMR}$  (DMSO- $d_6$ )  $\delta$  10.48 (s, 1H, NH), 7.99 (d,  $J$  = 0.5 Hz, 1H, CH = benzyldine), 7.20–7.14 (m, 1H, Ar-H), 7.10 (dd,  $J$  = 1.9, 0.5 Hz, 1H, Ar-H), 7.02 (d,  $J$  = 8.9 Hz, 1H, Ar-H), 6.01 (s, 2H), 4.25 (s, 2H, CH<sub>2</sub> dioxole), 2.79 (s, 3H).  $^{13}\text{C NMR}$  (DMSO- $d_6$ )  $\delta$  199.55, 168.79, 167.44, 165.66, 163.42, 157.52, 149.34, 148.33, 130.57, 128.22, 125.32, 122.05, 110.52, 109.65, 101.85, 35.90, 15.18. Anal. Calcd for C<sub>17</sub>H<sub>12</sub>N<sub>4</sub>O<sub>5</sub>S<sub>4</sub> (480): C, 42.50; H, 2.50; N, 11.66. Found: C, 42.45; H, 2.44; N, 11.62.

#### 2.1.3. 5-(Benzo[d][1,3]dioxol-5-ylmethylene)-3-(2-(2,4-dioxothiazolidin-3-yl)acetyl) Thiazolidine-2,4-dione (11)

The compound (**1**; 0.1 mol) was heated with (**4**; 0.1 mol) in DMF (30 mL) for 3 h. The reaction mixture was cooled, and the solid product was filtered off, dried, crystallized from DMF to give (**5**) as pale yellow crystals, yield 73%, m.p. > 300 °C. IR (KBr): ( $\nu/\text{cm}^{-1}$ ) = 1696, 1740 (CO).  $^1\text{H-NMR}$  (DMSO- $d_6$ )  $\delta$  7.99 (d,  $J$  = 0.4 Hz, 1H, CH = benzyldine), 7.20–7.14 (m,

1H, Ar-H), 7.10 (dd,  $J = 1.9, 0.5$  Hz, 1H, Ar-H), 7.02 (d,  $J = 8.9$  Hz, 1H, Ar-H), 6.01 (s, 2H, dioxole ring), 4.96 (s, 2H), 3.82 (s, 2H, thiazolidinone).  $^{13}\text{C}$  NMR (DMSO- $d_6$ )  $\delta$  177.61, 172.56, 167.67, 166.89, 165.73, 149.34, 148.33, 130.68, 128.22, 125.32, 122.05, 110.52, 109.65, 101.85, 43.92, 31.65. Anal. Calcd. for  $\text{C}_{16}\text{H}_{10}\text{N}_2\text{O}_7\text{S}_2$  (406): C, 47.29; H, 2.46; N, 6.89. Found: C, 47.24; H, 2.42; N, 6.85.

## 2.2. Computational Study

### 2.2.1. Preparation of the Small Molecule

The target compounds were built, and their energy was minimized with PM3 through MOPAC [29] then the DFT using B3LYP/6-311G \* was applied (Supplementary Materials).

### 2.2.2. Protein Selection and Molecular Docking

Docking experiment was carried out on the target active sites for *PPAR- $\gamma$*  (ID: 2PRG) and  $\alpha$ -amylase (ID: 2QV4) using MOE-2019. The inhibitors complexed with the crystal structures of *PPAR- $\gamma$*  (ID: 2PRG) and  $\alpha$ -amylase (ID: 2QV4) were obtained. Water and inhibitors were removed, then H-toms were supplemented by MOE-2019 suite tool, which was used to handle the kinase (pH = 7.4). All the ligands were fitted into the suitable binding sites. Formerly, the receptors were created with a parametric cubic-box (12 Å  $\times$  12 Å  $\times$  12Å) over a centroid-binding pocket. The other docking procedures are described in Supplementary Materials.

## 2.3. Biological Study

### 2.3.1. Animals

Healthy male albino Wistar rats (150  $\pm$  20 g) have been obtained as mentioned in Supplementary Materials.

### 2.3.2. Induction of Diabetes

The animals were kept fasting overnight (12 h) before induction of diabetes, which was induced in rats as reported [30–34] and mentioned in Supplementary Materials.

### 2.3.3. Determination of the Blood Glucose Levels

We obtained the blood samples from the tail vein of all rats, the blood-glucose-level “BGLs” were measured and monitored in all treatment groups at days 0 (basal), 2th, 4th, 15th, and 30th as reported [35].

### 2.3.4. Biochemical Analysis

The blood samples (0.5 mL) were withdrawn from the retro-orbital plexus of each rat and the other steps adapted for measuring the biochemical analysis are shown in (Supplementary Materials).

### 2.3.5. The In Vitro Inhibition of $\alpha$ -Amylase Assay

The  $\alpha$ -amylase activity of the probe compounds determined using a method [36].

### 2.3.6. DPPH Radical Scavenging Activity

The assay of 2,2-Diphenyl-1-picrylhydrazyl radical (DPPH) was performed according to the method at [37].

### 2.3.7. Statistical Analysis

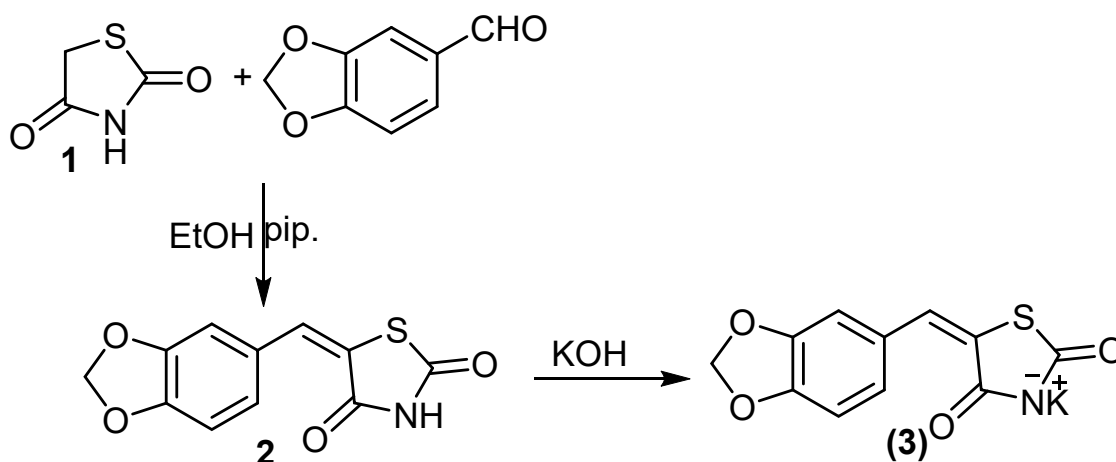
The analysis of the data is described in Supplementary Materials.

## 3. Results and Discussion

### 3.1. Chemistry

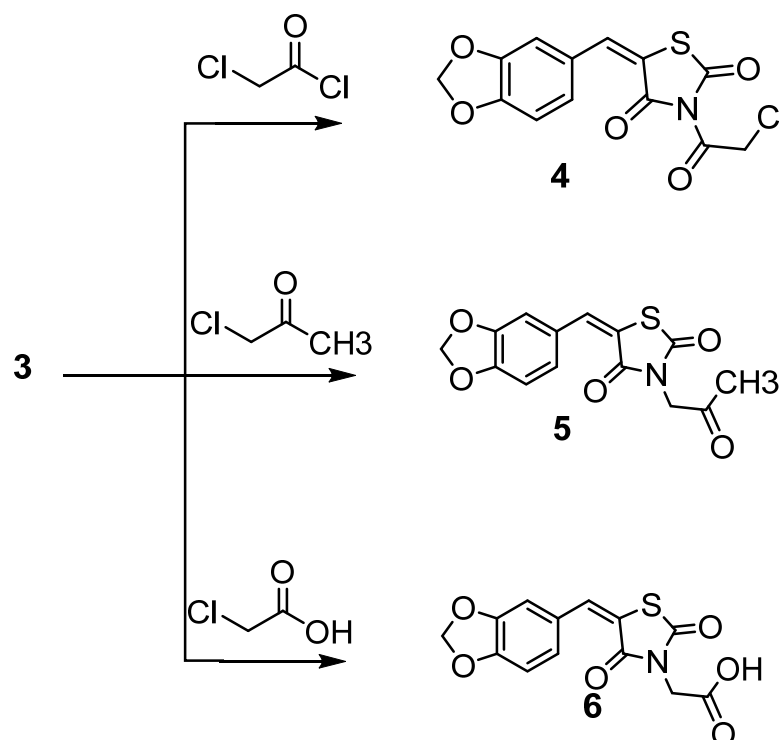
In a continuation of our previous work [37], we reported the synthesis of novel antidiabetic agents based on the thiazolidinedione scaffold. The 5-(benzo[d][1,3]dioxol-5-ylmethylene)

thiazolidine-2,4-dione reacted with potassium hydroxide in DMF to give the potassium salt derivative (3), Scheme 1.



Scheme 1. Synthesis of compounds 3.

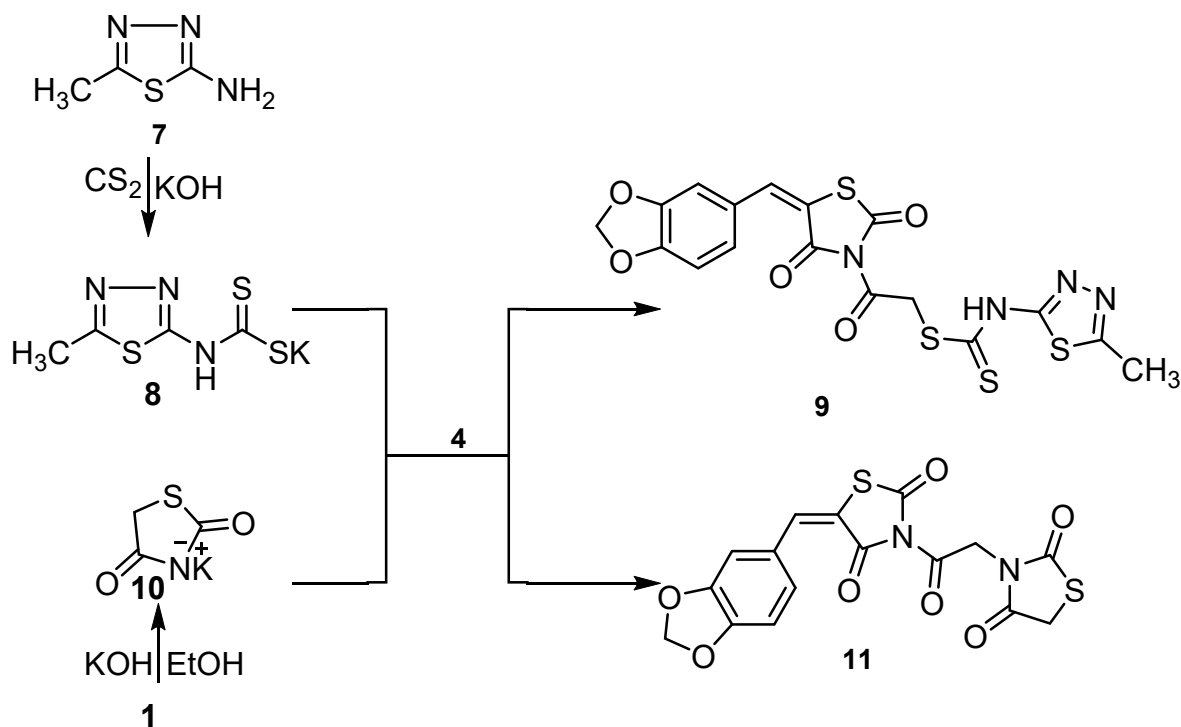
The molecule 3 underwent a further reaction with chloro-acetyl chloride to give chloroacetyl thiazolidine-2,4-dione 4 [37]. The interaction of the equimolar of potassium salt 3 with chloroacetone in DMF under a reflux condition afforded a 5-(benzo[d][1,3]dioxol-5-yl)methylene-3-(2-oxopropyl)thiazolidine-2,4-dione (5), Scheme 2. In the same manner, the potassium salt (3) reacted with chloroacetic acid to give 2-(5-(benzo[d][1,3]dioxol-5-yl)methylene)-2,4-dioxothiazolidin-3-yl) acetic acid (6) in good yield, Scheme 2.



Scheme 2. Synthesis of compounds 4–6.

Compound (4) was heated with potassium (5-methyl-1,3,4-thiadiazol-2-yl)-carbamodithioate (7) in DMF under stirring condition to give 2-(5-(benzo[d][1,3]dioxol-5-yl)methylene)-2,4-dioxothiazolidin-3-yl)-2-oxoethyl (5-methyl-1,3,4-thiadiazol-2-yl)-carbamodithioate 9, which displayed two absorption bands attributed to 2 C = O at 1698 and 1742  $\text{cm}^{-1}$ . The  $^1\text{H}$  NMR spectrum ( $\text{DMSO-d}_6$ ) of 9 revealed signals at  $\delta = 2.79$  (s, 3H,  $\text{CH}_3$ ), 3.60 (s, 2H,  $\text{CH}_2$ ),

4.25 (s, 2H, CH<sub>2</sub> of dioxole ring) and 10.48 (s, 1H, NH). Compound **4** interacted with the potassium 2,4-dioxothiazolidin-3-ide (**10**) to give 5-(benzo[d][1,3]dioxol-5-ylmethylene)-3-(2-(2,4-dioxothiazolidin-3-yl)acetyl)-thiazolidine-2,4-dione (**11**), Scheme 3. The IR spectrum (cm<sup>-1</sup>) of **11** revealed the absorption band at 1696 and 1740 cm<sup>-1</sup> for the two (C = O) group. The <sup>1</sup>H NMR spectrum (DMSO-d<sub>6</sub>) of **11** revealed signals at  $\delta$  = 3.82 (s, 2H, CH<sub>2</sub>), 4.96 (s, 2H, CH<sub>2</sub>), 6.01 (s, 2H, CH<sub>2</sub> of dioxole ring), 7.99 (s, 1H, CH = benzylidene).



**Scheme 3.** Synthesis of compounds **9** and **11**.

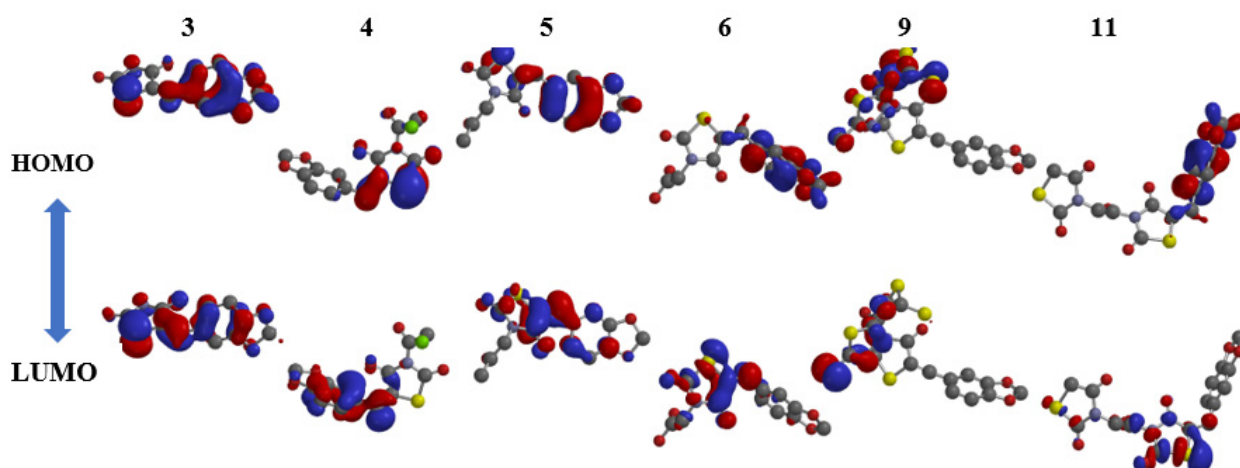
### 3.2. Molecular Modeling Studies

#### 3.2.1. Kinase Inter-/Intramolecular Interaction Stability Based on FMO Analysis

The DFT (density function theory) optimized the (**3–6**, **9**, **11**) hybrids using the B3YLP/6311G \*\* correlation function [38]. In all compounds, the thiazolidine-2,4-dione was stabilized with benzo[d][1,3]dioxole by planarity and/or coplanarity modes. The frontier molecular orbital “FMO” was defined as HOMO and LUMO (donating electron/accepting electron), respectively. These orbitals can decide the interaction route with the kinase. FMO gap and chemical reactivity determined the kinetic stability of the molecule [39]. The increasing energy level of HOMO compounds reflected their potent ability for providing the electron and more susceptible to oxidation, and vice versa [40,41].  $E_{\text{HOMO}}$  arranged the compounds in decreasing order **5** > **4** > **6** > **9** > **11** > **3** (Table 1). The HOMO sector is localized over thiazolidine-2,4-dione rings in compounds **3–5** and **9**. These compounds bear a LUMO area over benzodioxol ring. Inversely, the compound **11** has a HOMO area over benzodioxol and LUMO area covered thiazolidinedione (Figure 2).

**Table 1.** Calculated energetic reactivity parameters for compounds (3, 5–12) at DFT with B3LYP\6-311G \* Basics set.

	3	4	5	6	9	11		3	4	5	6	9	11
HOMO	−8.18	−6.839	−8.56	−8.93	−8.81	−9.23	$\mu^+$	−2.99	−1.79	−2.972	−3.345	−3.245	−3.35
LUMO	−1.26	−0.108	−1.11	−1.35	−1.39	−1.39	$\mu^-$	−6.45	−5.16	−6.697	−7.035	−6.955	−7.027
$\Delta G$	−6.92	−6.731	−7.45	−7.58	−7.42	−7.84	$\omega^-$	6.11	3.95	6.21	6.529	6.519	6.741
IP	8.18	6.839	9.23	8.93	8.81	8.56	$\omega^+$	2.786	1.37	2.672	3.011	3.041	3.106
A	1.26	0.108	1.11	1.35	1.39	1.39	$\omega^\pm$	8.798	5.32	8.693	9.58	9.56	9.847
$\eta$	3.46	3.365	3.725	3.79	3.71	3.92	$\Delta N_{\max}$	−0.682	1.03	−0.648	−0.678	−0.687	−0.677
S	0.289	0.297	0.268	0.263	0.269	0.255	$\Delta E_{\max}^{GS}$	2.728	−1.53	2.595	2.712	2.06	2.709
$\chi$	−4.72	−3.473	−4.835	−5.14	−5.1	−5.31	$\Delta E_{\max}^{VS}$	−0.682	−0.84	−0.648	−0.678	−0.687	−0.677
$\omega_i$	3.219	3.453	3.137	3.485	3.505	3.596							

**Figure 2.** HOMO and LUMO density of compounds (3, 5–12).

The negative energy values for HOMO and LUMO indicated that the intramolecular charge transfer from the thiazolidine-2,4-dione to benzodioxole corners occurred in 3–6 and 9. This direction was reversed in 11 molecule.

The energy gap  $\Delta G$  is a vital parameter for examining the stability of the biomolecule in the receptor.  $\Delta G$  is inversely linked with the binding interaction between ligand and receptor. The low value of  $\Delta G$  for the compound postulated a good binding interaction between their FMOs and the receptor of the kinase [40].

We computed the chemical reactivity descriptors for the molecules in (Table 1), such as: S, softness (measures the stability of the molecule which direct proportional with chemical reactivity) [42];  $\eta$ , hardness (the reciprocal of softness);  $\chi$ , electronegativity strength [43];  $\mu^-$ , the electron donation power;  $\mu^+$ , the potency for catching the electron;  $\omega^-$ , the electrodonation capacity;  $\omega^+$ , the electro-acceptance capacity;  $\omega^\pm$ , the net electrophilicity (measure the relative power between electron acceptance and electron donation) [44];  $\omega_i$ , the electrophilicity index in the ground state (studying the decreasing energy got from the donor  $\rightarrow$  acceptor movement) [45]. These parameters were represented in terms of I; the ionization potential and A; the electron affinity [44]. All the previous terms were calculated as reported [46,47].

The charge transfer examined the reactivity index term, " $\Delta N_{\max}$ ", which measured the stabilization energy when the system gains an additional charge from the environment (Table 1). The total binding energy measured the maximal electron transfer in the ground and valance states and represented in terms: " $\Delta E_{\max}^{GS}$ " and " $\Delta E_{\max}^{VS}$ " (Table 1). This work examined the electrophiles and nucleophiles based on both soft and hard terms.

The soft nucleophiles and hard electrophiles related to  $\Delta G$ , that can measure the stability index. The molecule with low  $\Delta G$  has high polarizability, softness, chemical reactivity, and nucleophilicity (thereby easily offering electrons to kinase) and vice versa. Table 1 showed the low softness values ( $\sim 0.250 - 0.296$  eV) for the (3–6, 9, 11) compounds, that may join to form a high degree of reactivity to the biological environment.

All (3–6, 9, and 11) compounds showed a similar value via ( $\omega^+$ ), ( $\mu^+$ ), and ( $\omega^+$ ) and were arranged as, bithiazolidinones 11 > free acid 6 > thioester 9 > acetyl 5 > potassium salt 3 > 4 (Table 1). The previous order reversed for electron donating behaviors ( $\mu^-$ ,  $\omega^-$ ). The data in (Table 1) proved that the molecular skeleton bearing di-thiazolidine-2,4-dione rings 11, thioester 9, and carboxyl group 6, can improve the obtaining of an electron from the kinase. Compounds 6, 9, 11 have the highest range of net electrophilicity ( $\omega \pm = 9.847$  to 9.58 eV). Thus, these compounds have promising electrophilicity, that may enhance the attacking chance over a polar active site of the receptor. In addition, our studies [48,49] showed a direct relationship between antioxidant ability and IP, with the former increasing as the latter's value decreases. The antioxidant molecule can convert the electron into a stable cationic free radical that promotes healthier radical scavenging via a one-electron transfer mechanism [48]. As reported [50], the antioxidant ability increased with decreasing IP value. Thus, the investigated compounds 3–6, 9, 11 displayed promising antioxidant activity. Based on the above data, all of the calculated descriptors for 3–6, 9, 11 were harmonized with the reported value for several biomaterials [51,52].

### 3.2.2. Molecular Electrostatic Potential (MEP)

The DFT plotted the molecular electrostatic potential (MEP) in (Figure 3) for the (3–6, 9, 11) compounds. The MEP figured a balance between the repulsive interaction attributed to nucleophilic ability, and attractive interactions related to electrophilic reactivity. The orange, yellow, and red areas depicted negative power (great electron density area). The blue shift figured a positive potential, while green color represented an intermediate potential ability. The MEPs showed a high level of electron density (showed in red color) covered over most of the backbone of the 3–5, 9, and 11 compounds. The red regions indicated electrophilic potency. We explained the variation in shading for the MEPs by the diversity of the electrostatic potential values. That was attributed to substrate  $\rightarrow$  receptor identification and caused the electrostatic interactions ability to expand [53].

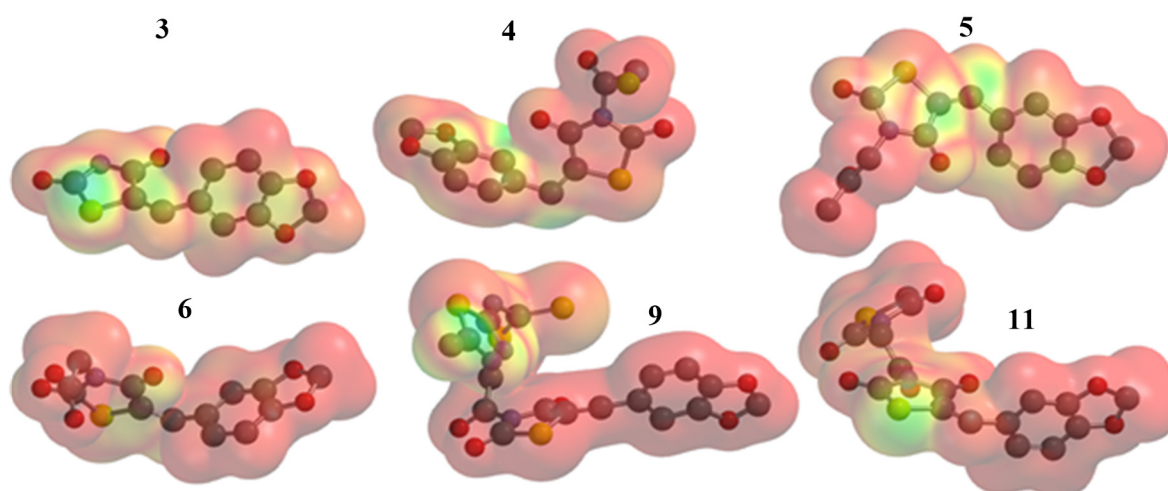


**Figure 3.** Plotted MEP of synthesized compounds (3–6, 9, and 11).

### 3.3. Docking Study

The molecular docking study targeted a PPAR- $\gamma$  and  $\alpha$ -amylase to examine a mode of regulation action for the investigated compounds. The ligand–protein interaction behavior was estimated based on the gold score function as implemented in MOE.2019 [54]. The probe compounds were successfully docked into the reported active sites (CYS 285, GLu233,



HIS 449, SER299, HIS323, CYS285, ASP300, Arg195) and (Asp300, Glu233 and Asp197) for (PPAR- $\gamma$ , PDB: 2PRG [55]) and ( $\alpha$ -amylase, PDB:2QV4 [56]), respectively.

The **3–6, 9, and 11** ligands were complexed successfully over the active sites, then minimized using the (MMFF94) force field. The highest MOE scoring function with the lowest RMSD was applied to evaluate the binding efficiency BE for the investigated compounds (Table 2).

**Table 2.** Docking energy scores (kcal/mol) derived from the MOE for (**3–6, 9, and 11**).

Cpd.	Ref.Inhibitor	3	4	5	6	9	11
PPAR- $\gamma$ (PDB: 2PRG)							
$\Delta E$	−7.86	−9.80	−6.48	−11.85	−9.14	−11.40	−9.01
RMSD	1.95	1.60	1.50	1.33	1.79	1.77	1.89
$E_{\text{-place}}$	−47.36	−112.41	−39.25	−37.56	−59.86	−89.46	−118.45
$E_{\text{-Int.}}$	−35.63	−30.39	−33.70	−32.85	−34.63	−38.27	−33.03
$E_{\text{-H.B.}}$	−0.25	−1.33	0.29	−0.65	−0.12	0.37	−0.23
LE	4.03	6.76	4.34	8.88	5.11	6.46	4.76
Ki( $\mu\text{M}$ )	1.39	1.70	2.21	1.61	1.87	1.65	1.88
LE <sub>scale</sub>	2.67	2.84	2.90	3.00	2.74	2.75	2.69
FQ	1.36	3.92	1.44	5.88	2.37	3.70	2.07
$\alpha$ -amylase, (PDB:2QV4)							
$\Delta E$	−5.59	−6.23	−6.50	−6.74	−6.14	−7.66	−6.33
RMSD	1.79	0.93	1.33	1.95	1.95	1.19	1.37
$E_{\text{-place}}$	−26.39	−43.10	−62.93	−23.29	15.12	−113.81	−37.51
$E_{\text{-Int.}}$	−32.26	−24.52	−19.04	−24.48	−15.75	−26.46	−18.00
$E_{\text{-H.B.}}$	−17.58	−15.46	−10.35	−11.87	−10.07	−11.36	−10.01
LE	3.12	6.67	4.89	3.46	3.15	6.44	4.61
Ki( $\mu\text{M}$ )	1.14	2.25	2.21	2.17	2.27	2.05	2.24
LE <sub>scale</sub>	−2.74	−3.31	−3.00	−2.67	−2.67	−3.10	−2.97
FQ	0.38	3.36	1.89	0.79	0.48	3.34	1.64

$\Delta E$ : free binding energy of ligand-pose which derived from gold tool, RMSD; the root mean square deviation of the docking pose compared to the co-crystal ligand position,  $E_{\text{-place}}$ : free binding energy of ligand-receptor.  $E_{\text{-Int.}}$ : binding-affinity energy of ligand-receptor,  $E_{\text{-H.B.}}$ : energy H-bonding between protein and ligand.

We calculated the inhibition constant (Ki) for further validation of the BE [57]. The bioactivity factor was also examined as the ligand-efficiency (LE) and fit-quality (FQ) [58]. All the synthesized compounds showed a BE higher than reference inhibitors (−7.86 and −5.59 kcal/mol) for PPAR- $\gamma$  and  $\alpha$ -amylase respectively (Table 2).

In PPAR- $\gamma$ : The compounds (**5** and **9**) exhibited the highest BE (−11.85 and −11.40 kcal/mol), with promising Ki (1.61 and 1.65  $\mu\text{M}$ ), respectively (Table 2). The BE for the remaining hybrids were arranged according to **4** < **11** < **6** < **3**. All of the compounds showed a normal range of bioactivity parameters, such as Ki, LE, and FQ [59]. The **5** and **9** interacted into a binding site in an identical manner, through an important hydrogen bond with Cys285, which was arranged in a perpendicular mode with their compounds (Figure 4).

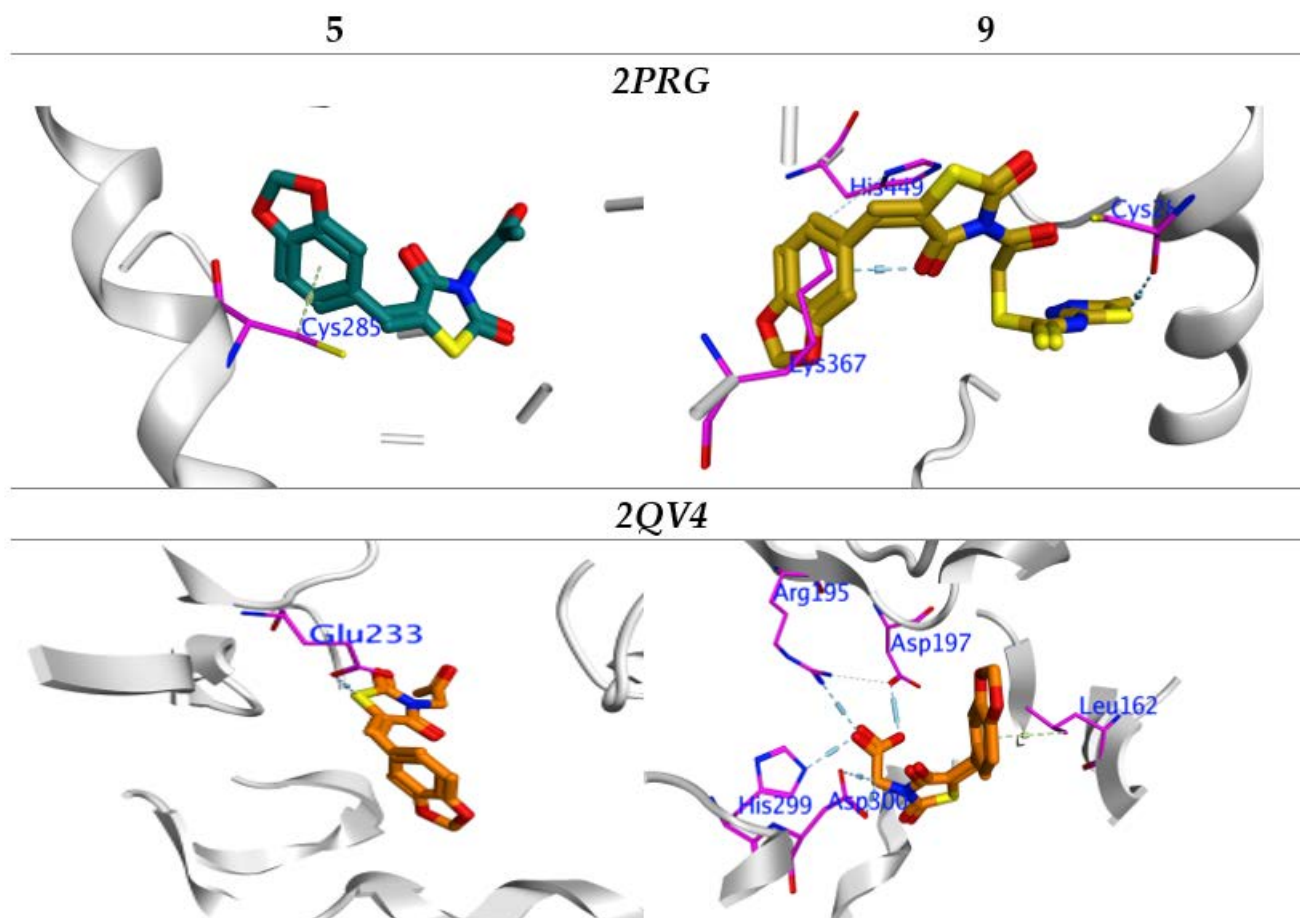


**Figure 4.** Interaction between ligands 5 and 9 with 2PRG and 2QV4 binding sites, which blue lines represented hydrogen bonding interaction.

In  $\alpha$ -amylase: The (5 and 9) also showed the most BE ( $-6.74$  and  $-7.66$  kcal/mol), with the lowest inhibition constant  $K_i$  ( $2.05$  and  $2.17$   $\mu\text{M}$ ), respectively (Table 2). The BE for other members is organized as  $4 < 6 < 3 < 11$ . All of the compounds showed a normal range of bioactivity parameters ( $K_i$ , LE, and FQ) [59]. Compound 5 formed H-bond with Glu233 residue, while compound 9 made H-bond with important amino acids Arg.195, ASP197, His.299, and Asp300, and also formed a  $\pi$ - $\pi$  interaction with backbone residue Leu.162 (Figure 4).

### 3.4. Biological Study

#### 3.4.1. The In Vitro $\alpha$ -Amylase Inhibitory Profile

This study examined the inhibitory potential for the (3–6, 9, and 11) compounds against  $\alpha$ -amylase enzyme. We applied six different concentrations (5,10,15,20,30, and 40)  $\mu\text{g}/\text{mL}$  for this test. These concentrations were plotted via the inhibition percentage to determine the  $\text{IC}_{50}$  (the concentration required to inhibit 50% of the enzyme) using the non-linear regression method. All of the tested compounds showed a marked inhibitory potential value about  $\text{IC}_{50} = 9.06$  to  $13.98$   $\mu\text{g}/\text{mL}$  compared to the “STD” standard drug (Acarbose)  $\text{IC}_{50} = 24.1$   $\mu\text{g}/\text{mL}$  (Figure 5). The compounds 5, 6, and 11 showed a higher inhibitory action than acarbose, with  $\text{IC}_{50} = 18.02$ ,  $10.26$ , and  $20.01$   $\mu\text{g}/\text{mL}$ . The 3 and 4 displayed moderate potency, with  $\text{IC}_{50} = (43.23$  and  $52.98$   $\mu\text{g}/\text{mL})$ , with significance ( $p < 0.05$ ) when compared to the positive control. Figure 5 shows that the parent compound with these fragments [acetyl (5), carboxy (6) and extra thiazaldinone (11)] in the corner increased the amount of activity. On the other hand, the inhibition potency decreased with the introduction of acetyl,

K salt (**3**), chloracetyl (**4**), and thiadiazole (**9**) to the molecular skeleton. We can explain the highest efficiency due to the increasing polarity feature in (**5** and **6**) and hydrophilicity in **11**, which can interact with the hydrophobic part of the active site.

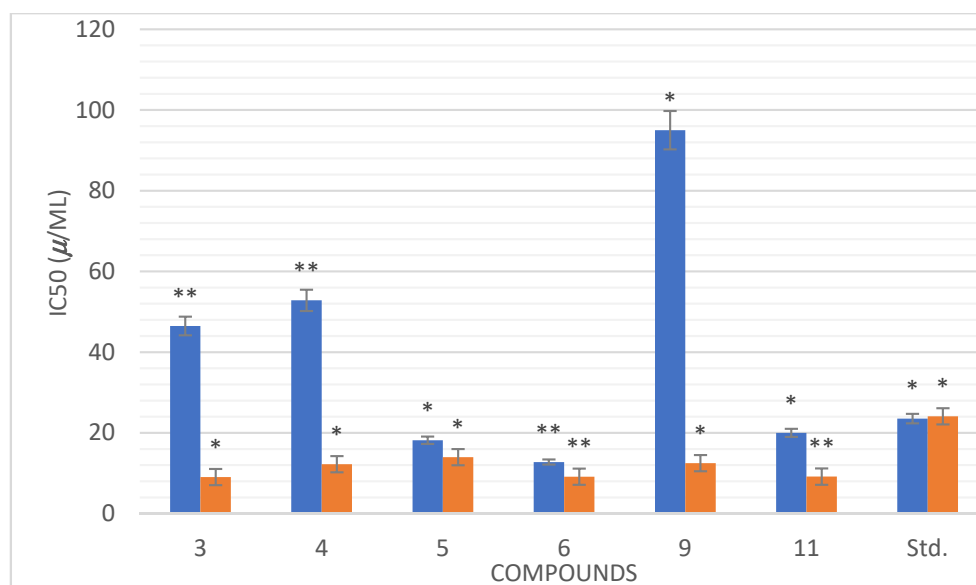


**Figure 5.** IC<sub>50</sub> in (µg/mL) for the tested compounds (**3–6**, **9**, and **11**) compared to ascorbic and acarbose, respectively, as standard drugs for DPPH radical (orange) and  $\alpha$ -amylase enzyme (blue), respectively. Data analyzed by one way ANOVA followed by LSD test and expressed as mean  $\pm$  SEM from five observations; \* represents change as compared to control; \*\* indicates  $p < 0.01$  and \* shows  $p < 0.05$ .

### 3.4.2. In Vitro Anti-Oxidant Activity

We examined the antioxidant activity of the (**3–6**, **9**, and **11**) hybrids using the stable DPPH assay [37]. The antioxidant result was represented as IC<sub>50</sub> (the concentration is essential for 50% reduction in the power of H-donation or radical scavenging). We estimated IC<sub>50</sub> based on different concentrations (0.16, 0.8, 4, 20, 40, 200, and 1000 µg/mL), as shown in Figure 5. All of the compounds showed a higher potency than Vitamin C and arranged Vit.C < **9** < **5** < **4** < **3** < **11** < **6**. Compounds **6** and **11** with the terminal carboxy and bi-thiazaldinone groups, respectively, showed the highest scavenging effect (IC<sub>50</sub> = 10.78 and 11.16 µg/mL). The increasing scavenging activity may be due to the stabilization of the lone pair in the conjugated system through the presence of the terminal carbonyl and thiazolidinone groups.

### 3.4.3. The In Vivo Regulation of Blood Glucose Level

This study used an alloxan-induced diabetic rat model to test the anti-hyperglycemic action of substances (**3–6**, **9**, **11**). Diabetes was successfully induced in the rats under investigation, as verified by raised their blood glucose level “BGL” compared with the normal control rats. The BGL was monitored for each tested compound at three different doses (50, 100, and 250 µ/Kg) and for five experimental period durations (0, 2, 4, 15, 30 days).

Compared with the control at 250 µ/Kg (Figure 6): all tested compounds (**3–6**, **9** and **11**) exhibited insignificant decrease in BGL compared to the normal group at pre-treatments. Compounds **5** and **11** showed promising decreases in BGL at the 15th and 30th treatments. Conversely, only compounds **6** and **11** at the 30th time duration of treatment showed a significant reduction in glucose level. At 100 µ/Kg in comparison with DC (Figure 6), the compounds (**4**, **6**, and **9**) exhibited moderate decreases in BGL at the 4th and 15th time durations, while compound **11** showed a significant reduction in glucose level at the 4th,

15th and 30th time durations. The results obtained from (Figure 6) showed a promising reduction in BGL at 50  $\mu$ /Kg with ( $p < 0.05$ ) for the treatment of compound 11 group without mortality during all the experiment periods compared to the DC group. The 4, 6 and 9 groups figured a moderate reduction in BGL value at 50  $\mu$ /Kg during most of the experimental periods at (4th,15th, and 30th). At 50  $\mu$ /Kg, we observed no mortality during any of the experiment periods for all tested compounds.

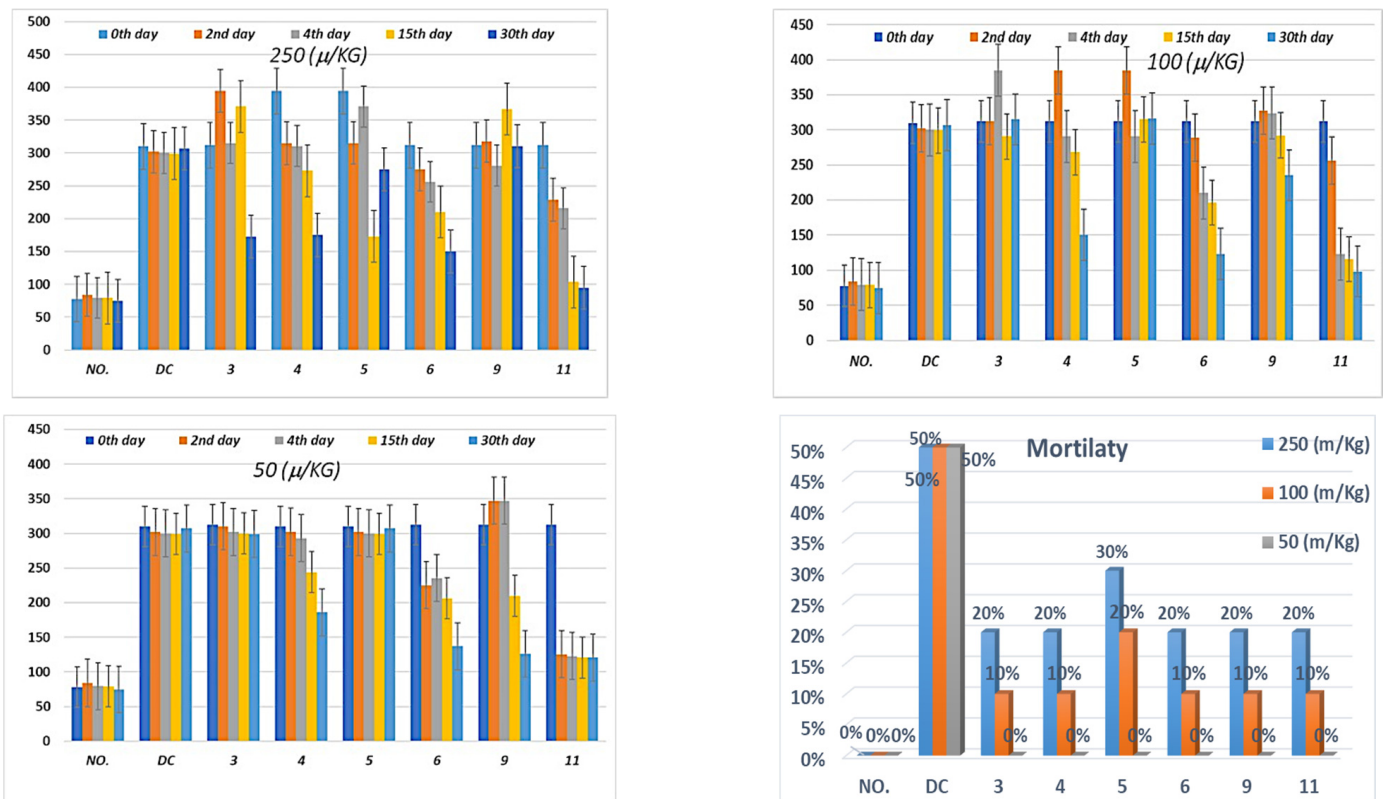


**Figure 6.** Antidiabetic effect and percent of mortality in three different concentration 50, 100, and 250 ( $\mu$ /Kg) at 0th day (pre-drug values), 2nd and 4th day (post-drug values) for each group of compounds (3–6, 9, 11) compared to diabetic-control “DC” and normal control “NO”. Data analyzed by one way ANOVA followed by LSD test and expressed as mean  $\pm$  SEM from five observations.

#### 3.4.4. Lipid Profile

A serious side effect related to diabetes is Hyperlipidemia [60,61]. Insulin deficiency promotes the adipocytes to generate a fatty acid, hepatic phospholipids and cholesterol [62]. Thus, we measured the levels of (cholesterol “CH”, triglyceride “TG”, high, low and very-low- and high/low and very low density lipoproteins “HDL, LDL and VLDL”) in serum for alloxan-loaded diabetes. Figure 7 showed the efficiency percentage for these parameters for the tested compounds and the normal control. All of the lipid parameters for compounds (3–6, 9, and 11) have ( $p < 0.05$ ) compared to the normal control group (Figure 7). The serum CH. Level decreased by 40%, 32%, 40%, 48%, 52%, and 43% for 3–6, 9, and 11, respectively, compared to the diabetic control group (Figure 7). The compounds 3–6, 9, and 11 shrank CH level nearly to a normal level of the control animals, on the 4th and 15th days. The 3, 5, 6, 9, and 11 groups showed a lower CH level than the normal animals, at the 30th day (Figure 7).

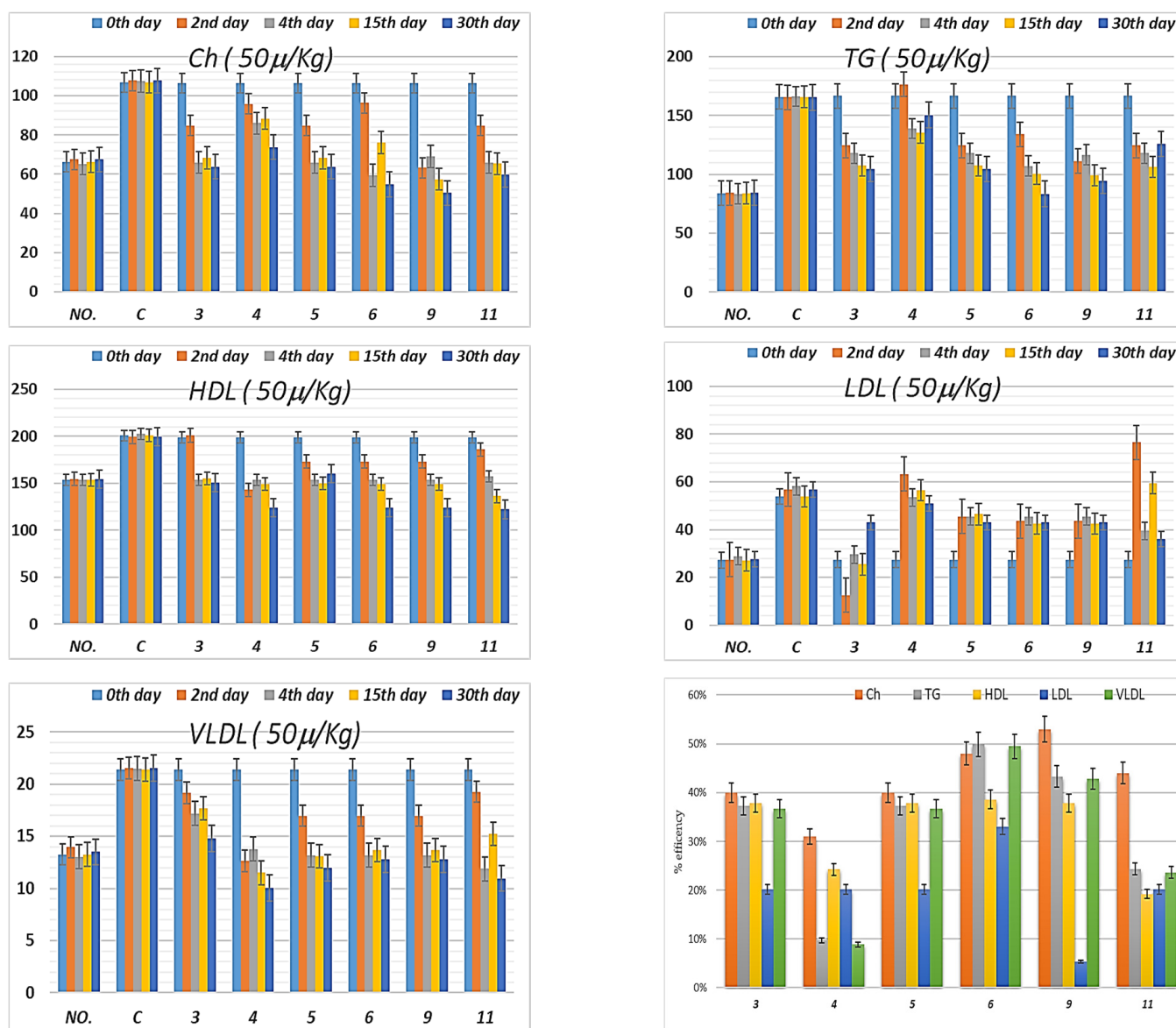


**Figure 7.** The level of Ch (cholesterol), TG (triglyceride), HDL (high density lipoprotein), LDL (low density lipoprotein) and VLDL (very low density lipoprotein) in serum of hyperglycemic loaded rats. 50 ( $\mu\text{g/Kg}$ ) on 0th day (pre-drug values), 2nd and 4th day (Post-drug values) for each group of compounds (3–6, 9, and 11) and control. Data analyzed by one way ANOVA followed by LSD test and expressed as mean  $\pm$  SEM from five observations.

On the contrary, the triglyceride level (TG) increased above the normal value when treated by the tested compounds. The TG level of alloxan-induced diabetes exceeded by 50.09% higher than the normal control animals throughout the experimental period (0th–30th days). The groups of compounds 3–6, 9, and 11 failed to regulate the TG level to the normal level, except for group 6, whose TG level decreased to the normal level (at the 30th day). All group members displayed lower TG level than the alloxan-induced diabetes control group, with a decreasing range of 9.69%–49.92% at the 30th day (Figure 7).

The HDL serum level for all of the groups improved compared to the normal control group at 15th days. All of the compounds significantly reduced the HDL value of infected rats by around 18% to 38%. The tested members successfully drove the HDL level of the infected rats to almost a normal HDL value during periods of the experiment (4th and 30th days).

In all periods of the experiment, the serum LDL level for all group members increased compared to that of the normal rats, with an LDL value range 15.12–78.25  $\mu$ /kg. Compound **3** can regulate the LDL value to the normal value on the 2nd and 15th days, but failed to do so on the 30th. Compared with the infected animals, all the compounds monitored LDL level lower than these rats for all periods, except (**4**) on 2nd and (**11**) 2nd and 15th days, with a reduction range of 5.35% to 35.58% (Figure 7). Molecule **4** displayed a VLDL level of serum below the normal value for all experimental periods compared to the normal rats. The **5**, **6**, and **9** groups regulated the VLDL level to the normal level on the 4th, 15th, and 30th days, while on 2nd day these compounds suffered from regulation the VLDL to normal level. Compound **11** regulated only the VLDL of infected rats to normal values on the 4th and 30th day. The group of **3** compound failed to reach to control value for VLDL at the 2nd to 15th days while, on 30th day, this group almost reached to the normal VLDL level.

### 3.5. In Silico Pharmacokinetic Profile

The oral bioavailability behaves as a vital role in the improvement of a therapeutic molecule. The MOE, and admet-SAR model simulated all descriptors. The obtained result is disclosed in (Table 3). The drug likeness was studied according to the Lipinski rule [63]. Table 3 showed that the tested compounds obeyed to their rule without violation, with a high absorption percentage (%ABS) in the range (66.7%–73.83%) [64]. The topological polar surface area (TPSA) for the tested compounds appeared promising, which was linked to good oral bioavailability properties [64].

**Table 3.** Drug likeness parameters and derived for **3**, **5**, **6**, **9**, and **11** ligands.

Cpd.	<b>3</b>	<b>5</b>	<b>6</b>	<b>9</b>	<b>11</b>
HBD	1	2	4	3	2
HBA	8	9	8	7	8
Log.P	2.83	3.21	2.25	2.42	2.74
Log.S	−5.53	−6.13	−5.73	−4.26	−5.11
V	0	0	0	0	0
TPSA	105.5	132.48	157.05	112.93	116.5
%ABS	72.6	73.83	66.7	70.03	68.8
Mutagenic	none	none	none	low	none
Tumorigenic	none	none	none	high	none
Reproductive Effective	none	none	none	high	none
Irritant	none	none	none	high	none

We investigated the carcinogenic effect (Figure 8), by comparing our structures with 981 various carcinogenic structures gained from the “Carcinogenic Potency Database (CPDB)”. The result exhibited that there is no carcinogenicity effect with the range of values (~0.6–0.9 mg/kg body wt./day). The synthesized compounds have a good oral bioavailability, high ability BBB transport, and no marked health effects observed for the rodent toxicity profiles.

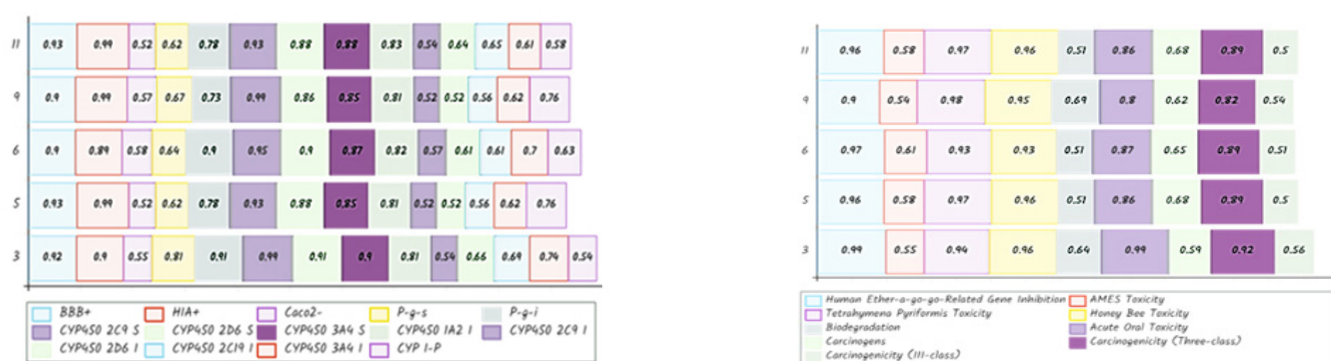


**Figure 8.** Absorption, distribution, and toxicity of pharmacokinetic parameters derived from the ADME-Tox for ligands (3, 5, 6, 9 and 11).

### 3.6. SAR Profile

The antihyperglycemic compounds, based on the thiazolidinedione scaffold were synthesized and characterized. The FMOs and global reactivity data indicated that the intramolecular charge transfer takes place between the thiazolidine-2,4-dione and benzodioxole corner in two directions. The MEP for these compounds represented that they have promising electrophilicity, that may enhance the attacking chance against the polar active site of the receptor. The molecular docking into the PPAR- $\gamma$  and  $\alpha$ -amylase showed the high binding affinity for the synthesized compounds, and may be a suitable regulator for both kinases. The in vitro inhibition potency via the  $\alpha$ -amylase was evaluated and represented that the parent compound bearing these corners acetyl (5), carboxyl (6), and thiazaldinone (11) is more efficient than acarbose. This efficacy decreased in the presence of K salt (3), acetyl chloride (4), and thiadiazole (11) in the molecular skeleton. All hybrids (3–6, 9, and 11) have a higher scavenging ability than Vitamin C. The molecular skeleton with K salt (3), carboxy (6), and bi-thiazaldinone (11) has a healthy antioxidant activity compared to the other members. The bi-thiazolidinone in (11) hybrid was the most potent regarding the regulation of BGL, Ch, TG, HDL, LDL, and VLDL levels at different concentrations at the 4th, 15th, and 30th days. All of the compounds enhanced the antihyperlipidemic effect compared to the DC. The antihyperglycemic efficiency improved with the introduction of an extra thiazolidinedione ring (11), or free carboxylic acid fragment (6) on the 4th, 15th, and 30th days compared to the DC. The in silico ADMET of the tested compounds showed a good oral bioavailability and high BBB transport ability. The rodent toxicity profile showed that no marked carcinogenic and non-healthy effect was observed for the synthesized compounds.

## 4. Conclusions

The new thiazolidinediones were synthesized and characterized. The FMOs and global reactivity data indicated that an intramolecular charge transfer occurs in two directions between the benzodioxole and thiazolidine-2,4-dione corners. The MEPs represented that they have promising electrophilicity, that may have enhanced the attacking chance over the polar active site of the receptor. The molecular docking simulation into the PPAR- $\gamma$  and  $\alpha$ -amylase displayed that the synthesized compounds may be a suitable regulator for both kinases. The inhibition potency via the  $\alpha$ -amylase in vitro showed that the compounds 5, 6, and 11 displayed the highest efficacy against acarbose and other compounds. Conversely, all of the compounds had a higher ability to scavenge radicals compared to Vitamin C. All of the compounds exhibited insignificant BGL pre and post the experimental periods compared to NO and DC, while, after the 30th treatments, they successfully decreased the BGL for all concentrations. None of the compounds exhibited any mortality at 50  $\mu\text{g}/\text{mL}$  for all experiment durations. Moreover, all the compounds at 50  $\mu\text{g}/\text{Kg}$  enhanced the antihyperlipidemic effect compared to the normal level. ADMET profile in silico for these

compounds displayed a promising oral bioavailability and BBB transport ability without any discernible carcinogenic or non-healthy effects in rodents.

**Supplementary Materials:** The following are available online at <https://www.mdpi.com/article/10.3390/biomedicines10010024/s1>, Figure S1: superimpose for the most active compounds.

**Author Contributions:** Project administration, M.Y.S., Conceptualization, M.Y.S. and A.A.E.; methodology, M.M.A., H.S.N. and M.M.K.; software, A.A.E. and S.A.A.; validation, M.M.A. and A.A.E.; formal analysis, A.A.E.; investigation, M.Y.S.; resources, M.M.A.; data curation, H.S.N.; writing—original draft preparation, A.A.E.; writing—review and editing, A.A.E.; visualization, A.A.E.; supervision, A.A.E. All authors have read and agreed to the published version of the manuscript.

**Funding:** This work was supported financially by the Deanship of Scientific Research at Umm Al-Qura University to Manal Semih (Grant Code: 18-SCI-1-03-0012).

**Institutional Review Board Statement:** The study was conducted according to the guidelines of the declaration of Helsinki and approved by the national research center in Egypt.

**Informed Consent Statement:** Not applicable.

**Data Availability Statement:** Data Available in “MDPI Research Data Policies” at <https://www.mdpi.com/ethics> (accessed on 25 October 2021).

**Acknowledgments:** The authors would like to thank the Deanship of Scientific Research at Umm Al-Qura University for the continuous support.

**Conflicts of Interest:** The authors declare no conflict of interest.

## References

1. Zimmet, P.; Alberti, K.G.; Shaw, J. Global and societal implications of the diabetes epidemic. *Nature* **2001**, *414*, 782–787. [[CrossRef](#)] [[PubMed](#)]
2. Wild, S.H.; Roglic, G.; Green, A.; Sicree, R.; King, H. Global prevalence of diabetes: Estimates for the year 2000 and projections for 2030: Response to Rathman and Gian. *Diabetes Care* **2004**, *27*, 2569. [[CrossRef](#)]
3. Bhutani, R.; Pathak, D.P.; Kapoor, G.; Husain, A.; Kant, R.; Iqbal, M.A. Synthesis, Molecular modelling studies and ADME prediction of benzothiazole clubbed oxadiazole-Mannich bases, and evaluation of their Anti-diabetic activity through in-vivo model. *Bioorganic Chem.* **2018**, *77*, 6–15. [[CrossRef](#)] [[PubMed](#)]
4. Cho, N.H.; Shaw, J.E.; Karuranga, S.; Huang, Y.; da Rocha Fernandes, J.D.; Ohlrogge, A.W.; Malanda, B. IDF Diabetes Atlas: Global estimates of diabetes prevalence for 2017 and projections for 2045. *Diabetes Res. Clin. Pract.* **2018**, *138*, 271–281. [[CrossRef](#)]
5. Diamond, J. The double puzzle of diabetes. *Nature* **2003**, *423*, 599–602. [[CrossRef](#)] [[PubMed](#)]
6. King, H.; Aubert, R.E.; Herman, W.H. Global burden of diabetes, 1995–2025: Prevalence, numerical estimates, and projections. *Diabetes Care* **1998**, *21*, 1414–1431. [[CrossRef](#)]
7. Del Prato, S.; Chilton, R. Practical strategies for improving outcomes in T2DM: The potential role of pioglitazone and DPP4 inhibitors. *Diabetes Obes. Metab.* **2018**, *20*, 786–799. [[CrossRef](#)] [[PubMed](#)]
8. American Diabetes, A. Pharmacologic approaches to glycemic treatment: Standards of Medical Care in Diabetes—2019. *Diabetes Care* **2019**, *42* (Suppl. S1), S90–S102. [[CrossRef](#)]
9. Tangphatsornruang, S.; Naconsie, M.; Thammarongtham, C.; Narangajavana, J. Isolation and characterization of an  $\alpha$ -amylase gene in cassava (*Manihot esculenta*). *Plant Physiol. Biochem.* **2005**, *43*, 821–827. [[CrossRef](#)] [[PubMed](#)]
10. Sales, P.M.; Souza, P.M.; Simeoni, L.A.; Magalhães, P.O.; Silveira, D.  $\alpha$ -Amylase inhibitors: A review of raw material and isolated compounds from plant source. *J. Pharm. Pharm. Sci.* **2012**, *15*, 141–183. [[CrossRef](#)]
11. Feng, J.; Lu, Y.; Cai, Z.F.; Zhang, S.P.; Guo, Z.R. Design, synthesis and in vitro evaluation of a series thiazolidinediones analogs as PPAR modulators. *Chin. Chem. Lett.* **2007**, *18*, 45–47. [[CrossRef](#)]
12. Brownlee, M. Biochemistry and molecular cell biology of diabetic complications. *Nature* **2001**, *414*, 813–820. [[CrossRef](#)]
13. Brownlee, M. The pathobiology of diabetic complications. *Diabetes* **2005**, *54*, 1615–1625. [[CrossRef](#)] [[PubMed](#)]
14. Brownlee, M.; Hirsch, I.B. Glycemic variability: A hemoglobin A1c-independent risk factor for diabetic complications. *JAMA* **2006**, *295*, 1707–1708. [[CrossRef](#)]
15. Chiasson, J.L.; Josse, R.G.; Gomis, R.F.; Hanefeld, M.; Karasik, A.; Laakso, M. Acarbose for the prevention of Type 2 diabetes, hypertension and cardiovascular disease in subjects with impaired glucose tolerance: Facts and interpretations concerning the critical analysis of the STOP-NIDDM Trial data. *Diabetologia* **2004**, *47*, 969–975. [[CrossRef](#)]
16. Yokoyama, H.; Katakami, N.; Yamasaki, Y. Recent advances of intervention to inhibit progression of carotid intima-media thickness in patients with type 2 diabetes mellitus. *Stroke* **2006**, *37*, 2420–2427. [[CrossRef](#)]
17. Davidson, M.A.; Mattison, D.R.; Azoulay, L.; Krewski, D. Thiazolidinedione drugs in the treatment of type 2 diabetes mellitus: Past, present and future. *Crit. Rev. Toxicol.* **2018**, *48*, 52–108. [[CrossRef](#)]



18. Xiao, B.; Xiao, Y.; Ning, H.; Han, X.; Li, W.; Ma, Y.; Zhao, N.; Du, G.; Dong, Y.; Jung, J.H. In vitro dual-target activities and in vivo antidiabetic effect of 3-hydroxy-N-(p-hydroxy-phenethyl) phthalimide in high-fat diet and streptozotocin-induced diabetic golden hamsters. *Med. Chem. Res.* **2020**, *29*, 2077–2088. [[CrossRef](#)]
19. Khatoon, H.; Najam, R. Effects of Rosiglitazone and Acarbose (with and without Cornstarch Diet) on serum electrolytes in diabetic rats. *J. Appl. Pharm. Sci.* **2012**, *2*, 50. [[CrossRef](#)]
20. Bennett, W.L.; Maruthur, N.M.; Singh, S.; Segal, J.B.; Wilson, L.M.; Chatterjee, R.; Marinopoulos, S.S.; Puhan, M.A.; Ranasinghe, P.; Block, L. Comparative effectiveness and safety of medications for type 2 diabetes: An update including new drugs and 2-drug combinations. *Ann. Intern. Med.* **2011**, *154*, 602–613. [[CrossRef](#)]
21. Sims, H.; Smith, K.H.; Bramlage, P.; Minguet, J. Sotagliflozin: A dual sodium-glucose co-transporter-1 and-2 inhibitor for the management of Type 1 and Type 2 diabetes mellitus. *Diabet. Med.* **2018**, *35*, 1037–1048. [[CrossRef](#)]
22. Frias, J.P.; Nauck, M.A.; Van, J.; Kutner, M.E.; Cui, X.; Benson, C.; Urva, S.; Gimeno, R.E.; Milicevic, Z.; Robins, D.; et al. Efficacy and safety of LY3298176, a novel dual GIP and GLP-1 receptor agonist, in patients with type 2 diabetes: A randomised, placebo-controlled and active comparator-controlled phase 2 trial. *Lancet* **2018**, *392*, 2180–2193. [[CrossRef](#)]
23. Garcia-Vallvé, S.; Guasch, L.; Tomas-Hernández, S.; del Bas, J.M.; Ollendorff, V.; Arola, L.; Pujadas, G.; Mulero, M. Peroxisome Proliferator-Activated Receptor  $\gamma$  (PPAR $\gamma$ ) and Ligand Choreography: Newcomers Take the Stage: Miniperspective. *J. Med. Chem.* **2015**, *58*, 5381–5394. [[CrossRef](#)] [[PubMed](#)]
24. May, L.D.; Lefkowitz, J.H.; Kram, M.T.; Rubin, D.E. Mixed hepatocellular–cholestatic liver injury after pioglitazone therapy. *Ann. Intern. Med.* **2002**, *136*, 449–452. [[CrossRef](#)]
25. Okumura, T. Mechanisms by which thiazolidinediones induce anti-cancer effects in cancers in digestive organs. *J. Gastroenterol.* **2010**, *45*, 1097–1102. [[CrossRef](#)] [[PubMed](#)]
26. Devji, T.; Reddy, C.; Woo, C.; Awale, S.; Kadota, S.; Carrico-Moniz, D. Pancreatic anticancer activity of a novel geranylgeranylated coumarin derivative. *Bioorg. Med. Chem. Lett.* **2011**, *21*, 5770–5773. [[CrossRef](#)] [[PubMed](#)]
27. Naim, M.J.; Alam, M.J.; Ahmad, S.; Nawaz, F.; Shrivastava, N.; Sahu, M.; Alam, O. Therapeutic journey of 2,4-thiazolidinediones as a versatile scaffold: An insight into structure activity relationship. *Eur. J. Med. Chem.* **2017**, *129*, 218–250. [[CrossRef](#)]
28. S Bahare, R.; Ganguly, S.; Agrawal, R.; N Dikshit, S. Thiazolidine: A Potent Candidate for Central Nervous System Diseases. *Cent. Nerv. Syst. Agents Med. Chem. Former. Curr. Med. Chem.-Cent. Nerv. Syst. Agents* **2017**, *17*, 26–29. [[CrossRef](#)]
29. Stewart, J.J. Optimization of parameters for semiempirical methods VI: More modifications to the NDDO approximations and re-optimization of parameters. *J. Mol. Model.* **2013**, *19*, 1–32. [[CrossRef](#)] [[PubMed](#)]
30. Fernandes, N.P.; Lagishetty, C.V.; Panda, V.S.; Naik, S.R. An experimental evaluation of the antidiabetic and antilipidemic properties of a standardized Momordica charantia fruit extract. *BMC Complementary Altern. Med.* **2007**, *7*, 29. [[CrossRef](#)]
31. Bodade, S.S.; Shaikh, K.S.; Kamble, M.S.; Chaudhari, P.D. A study on ethosomes as mode for transdermal delivery of an antidiabetic drug. *Drug Deliv.* **2013**, *20*, 40–46. [[CrossRef](#)]
32. Gandhi, G.R.; Sasikumar, P. Antidiabetic effect of Merremia emarginata Burm. F. in streptozotocin induced diabetic rats. *Asian Pac. J. Trop. Biomed.* **2012**, *2*, 281–286. [[CrossRef](#)]
33. Pareek, H.; Sharma, S.; Khajja, B.S.; Jain, K.; Jain, G. Evaluation of hypoglycemic and anti-hyperglycemic potential of *Tridax procumbens* (Linn.). *BMC Complementary Altern. Med.* **2009**, *9*, 48. [[CrossRef](#)]
34. Gadadare, R.; Mandpe, L.; Pokharkar, V. Ultra rapidly dissolving repaglinide nanosized crystals prepared via bottom-up and top-down approach: Influence of food on pharmacokinetics behavior. *AAPS PharmSciTech* **2015**, *16*, 787–799. [[CrossRef](#)] [[PubMed](#)]
35. Sharma, M.; Kohli, S.; Dinda, A. In-vitro and in-vivo evaluation of repaglinide loaded floating microspheres prepared from different viscosity grades of HPMC polymer. *Saudi Pharm. J.* **2015**, *23*, 675–682. [[CrossRef](#)] [[PubMed](#)]
36. Naem, F.; Nadeem, H.; Muhammad, A.; Zahid, M.A.; Saeed, A. Synthesis,  $\alpha$ -Amylase Inhibitory Activity and Molecular Docking Studies of 2,4-Thiazolidinedione Derivatives. *Open Chem. J.* **2018**, *5*, 134–144. [[CrossRef](#)]
37. Elhenawy, A.; Salama, A.A.; All, M.M.A.; Alomri, A.A.; Nassar, H. Synthesis, characterization and discovery novel anti-diabetic and anti-hyperlipidemic thiazolidinedione derivatives. *Int. J. Pharm. Sci. Rev. Res.* **2015**, *31*, 23–30.
38. Frisch, M.; Trucks, G.; Schlegel, H.; Scuseria, G.; Robb, M.; Cheeseman, J.; Scalmani, G.; Barone, V.; Mennucci, B.; Petersson, G. *Gaussian 09, Revision D. 01*; Gaussian, Inc.: Wallingford, CT, USA, 2013.
39. Hofmann, P. *Arvi Rauk: “Orbital Interaction Theory of Organic Chemistry”*; Wiley & Sons: New York, NY, USA, 1994. ISBN 0-471-59389-3. 307 Seiten, mit HMO—Programmdiskette, Preis: \$45.50. *Ber. Der Bunsenges. Für Phys. Chem.* **1995**, *99*, 997–999.
40. Fukui, K. Role of frontier orbitals in chemical reactions. *Science* **1982**, *218*, 747–754. [[CrossRef](#)]
41. Wildman, S.A.; Crippen, G.M. Prediction of physicochemical parameters by atomic contributions. *J. Chem. Inf. Comput. Sci.* **1999**, *39*, 868–873. [[CrossRef](#)]
42. Parr, R.G.; Chattaraj, P.K. Principle of maximum hardness. *J. Am. Chem. Soc.* **1991**, *113*, 1854–1855. [[CrossRef](#)]
43. Parr, R.G.; Pearson, R.G. Absolute hardness: Companion parameter to absolute electronegativity. *J. Am. Chem. Soc.* **1983**, *105*, 7512–7516. [[CrossRef](#)]
44. Lamaka, S.V.; Zheludkevich, M.L.; Yasakau, K.A.; Serra, R.; Poznyak, S.; Ferreira, M. Nanoporous titania interlayer as reservoir of corrosion inhibitors for coatings with self-healing ability. *Prog. Org. Coat.* **2007**, *58*, 127–135. [[CrossRef](#)]
45. Parr, R.G.; Szentpaly, L.V.; Liu, S. Electrophilicity index. *J. Am. Chem. Soc.* **1999**, *121*, 1922–1924. [[CrossRef](#)]

46. Elhenawy, A.A.; Al-Harbi, L.M.; El-Gazzar, M.A.; Khowdiary, M.M.; Moustfa, A. Synthesis, molecular properties and comparative docking and QSAR of new 2-(7-hydroxy-2-oxo-2H-chromen-4-yl)acetic acid derivatives as possible anticancer agents. *Spectrochim. Acta A Mol. Biomol. Spectrosc.* **2019**, *218*, 248–262. [CrossRef]
47. Elgendy, A.; Nady, H.; El-Rabiei, M.M.; Elhenawy, A.A. Understanding the adsorption performance of two glycine derivatives as novel and environmentally safe anti-corrosion agents for copper in chloride solutions: Experimental, DFT, and MC studies. *RSC Adv.* **2019**, *9*, 42120–42131. [CrossRef]
48. El Gaafary, M.; Syrovets, T.; Mohamed, H.M.; Elhenawy, A.A.; El-Agrody, A.M.; Amr, A.E.-G.E.; Ghabbour, H.A.; Almhizia, A.A. Synthesis, Cytotoxic Activity, Crystal Structure, DFT Studies and Molecular Docking of 3-Amino-1-(2, 5-dichlorophenyl)-8-methoxy-1H-benzo [f] chromene-2-carbonitrile. *Crystals* **2021**, *11*, 184. [CrossRef]
49. Al-Harbi, L.M.; Nassar, H.S.; Moustfa, A.; Alosaimi, A.M.; Mohamed, H.M.; Khowdiary, M.M.; El-Gazzar, M.A.; Elhenawy, A.A. Novel coumarin amino acid derivatives: Design, synthesis, docking, absorption, distribution, metabolism, elimination, toxicity (ADMET), quantitative structure–activity relationship (QSAR) and anticancer studies. *Mater. Express* **2020**, *10*, 1375–1394. [CrossRef]
50. Elhenawy, A.A.; Al-Harbi, L.M.; El-Gazzar, M.A.; Khowdiary, M.M.; Ouidate, A.; Alosaimi, A.M.; Elhamid Salim, A. Naproxenylamino acid derivatives: Design, synthesis, docking, QSAR and anti-inflammatory and analgesic activity. *Biomed. Pharm.* **2019**, *116*, 109024. [CrossRef]
51. Elhenawy, A.A.; Al-Harbi, L.M.; Moustafa, G.O.; El-Gazzar, M.A.; Abdel-Rahman, R.F.; Salim Abd Elhamid Drug Design. Development and Therapy, Synthesis, comparative docking, and pharmacological activity of naproxen amino acid derivatives as possible anti-inflammatory and analgesic agents. *Drug Des. Devel.* **2019**, *13*, 1773–1790. [CrossRef]
52. Elsisy, D.M.; Ragab, A.; Elhenawy, A.A.; Farag, A.A.; Ali, A.M.; Ammar, Y.A. Experimental and theoretical investigation for 6-Morpholinosulfonylquinoxalin-2 (1H)-one and its hydrazone derivate: Synthesis, characterization, tautomerization and antimicrobial evaluation. *J. Mol. Struct.* **2022**, *1247*, 131314. [CrossRef]
53. Luque, F.J.; López, J.M.; Orozco, M. Perspective on “Electrostatic interactions of a solute with a continuum. A direct utilization of ab initio molecular potentials for the prevision of solvent effects”. In *Theoretical Chemistry Accounts*; Springer: Berlin/Heidelberg, Germany, 2000; pp. 343–345.
54. Molecular Operating Environment (MOE). C.C.G.U., 1010 Handbook St. West, Suite 910; Montreal, QC, Canada, 2017. Available online: <https://www.chemcomp.com/Products.htm> (accessed on 25 October 2021).
55. Willson, T.M.; Brown, P.J.; Sternbach, D.D.; Henke, B.R. The PPARs: From orphan receptors to drug discovery. *J. Med. Chem.* **2000**, *43*, 527–550. [CrossRef]
56. Maurus, R.; Begum, A.; Williams, L.K.; Fredriksen, J.R.; Zhang, R.; Withers, S.G.; Brayer, G.D. Alternative Catalytic Anions Differentially Modulate Human  $\alpha$ -Amylase Activity and Specificity. *Biochemistry* **2008**, *47*, 3332–3344. [CrossRef]
57. Bohacek, R.S.; McMartin, C.; Guida, W.C. The art and practice of structure—Based drug design: A molecular modeling perspective. *Med. Res. Rev.* **1996**, *16*, 3–50. [CrossRef]
58. Hopkins, A.L.; Keserü, G.M.; Leeson, P.D.; Rees, D.C.; Reynolds, C.H. The role of ligand efficiency metrics in drug discovery. *Nat. Rev. Drug Discov.* **2014**, *13*, 105–121. [CrossRef] [PubMed]
59. Nguyet, T.T.; Dat, D.T.; Ha, N.V. Stereoelectronic Properties of 1,2,4-Triazole-Derived N-heterocyclic Carbenes—A Theoretical Study. *VNU J. Sci. Nat. Sci. Technol.* **2019**, *35*. [CrossRef]
60. Saravanan, R.; Pari, L. Antihyperlipidemic and antiperoxidative effect of Diasulin, a polyherbal formulation in alloxan induced hyperglycemic rats. *BMC Complementary Altern. Med.* **2005**, *5*, 14. [CrossRef] [PubMed]
61. Adam, S.H.; Giribabu, N.; Rao, P.V.; Sayem, A.S.M.; Arya, A.; Panichayupakaranant, P.; Korla, P.K.; Salleh, N. Rhinacanthin C ameliorates hyperglycaemia, hyperlipidemia and pancreatic destruction in streptozotocin–nicotinamide induced adult male diabetic rats. *Eur. J. Pharmacol.* **2016**, *771*, 173–190. [CrossRef] [PubMed]
62. Rajasekaran, S.; Ravi, K.; Sivagnanam, K.; Subramanian, S. Beneficial effects of Aloe vera leaf gel extract on lipid profile status in rats with streptozotocin diabetes. *Clin. Exp. Pharmacol. Physiol.* **2006**, *33*, 232–237. [CrossRef]
63. Lipinski, C.A.; Lombardo, F.; Dominy, B.W.; Feeney, P.J. Experimental and computational approaches to estimate solubility and permeability in drug discovery and development settings. *Adv. Drug Deliv. Rev.* **1997**, *23*, 3–25. [CrossRef]
64. Clark, D.E.; Pickett, S.D. Computational methods for the prediction of ‘drug-likeness’. *Drug Discov. Today* **2000**, *5*, 49–58. [CrossRef]